CrystEngComm

PAPER

View Article Online
View Journal | View Issue

Cite this: *CrystEngComm*, 2015, **17**, 3376

Vanadia directed synthesis of anatase TiO_2 truncated bipyramids with preferential exposure of the reactive {001} facet

Quanquan Shi, Yong Li,* Ensheng Zhan, Na Ta and Wenjie Shen*

Received 25th February 2015,
Accepted 24th March 2015

DOI: 10.1039/c5ce00385g

www.rsc.org/crystengcomm

Anatase TiO_2 truncated bipyramids that dominantly exposed the reactive {001} facet were hydrothermally synthesized using vanadia as the structure-directing agent. The exposed fraction of the {001} facet approached 53% upon adjusting the V/Ti molar ratio of the synthetic solution. Mechanistic investigation, together with control experiments, verified that vanadia stabilized the {001} facet and induced the construction of the truncated bipyramids. After calcination at 723 K in air, the resulting VO_x/TiO_2 truncated bipyramids effectively catalyzed the selective reduction of NO by ammonia.

Introduction

Morphology control of metal oxides for achieving preferential exposure of reactive crystal facets has received extensive attention in the past decades.[1–3] Tuning the shape of oxide-catalyst particles not only facilitates the development of advanced catalysts towards target reactions but also provides an in-depth understanding of their structure–reactivity relationship. In this context, anatase TiO_2 sets a typical example.[4–8] TiO_2 crystallizes as spindle-like particles and predominately exposes the thermodynamically stable {101} facet.[9–12] Because of the fast growth of the reactive {001} facet during synthesis, its exposure is usually no more than 10%.[13] Hydrothermal synthesis with the aid of F^- was proposed to be most effective in promoting the exposure of the {001} facet.[14–17] Theoretical calculations have confirmed that adsorption of F^- lowered the surface energy of the {001} facet and thus favored its preferential exposure.[14] With such a strategy, TiO_2 truncated bipyramids exposing 47% {001} facets were hydrothermally fabricated using hydrofluoric acid as the structure-directing agent.[14] Through optimization of the synthetic conditions, exposure of the {001} facet over TiO_2 nanosheets was further improved to a level of 98.7%.[15] It was found that F^- played dual roles in the fabrication of anatase TiO_2 hollow nanosheets that exposed 65% {001} facets; it directed the construction of the nanosheets through the formation of NH_4TiOF_3 as the key intermediate, and at the same time participated in the etching process to create the hollow structures.[16] However, the toxic and erosive nature of HF or F-containing compounds caused serious environmental problems during the liquid-phase synthesis. Moreover, the strongly adsorbed F^- on the obtained TiO_2 nanomaterials usually blocks the active sites and removal of these impurities requires extensive washing with aqueous NaOH solution.[18] Therefore, it is highly desirable to develop a fluorine-free approach to selectively expose the reactive {001} facet of TiO_2 nanoparticles.

Organic amines have been reported to induce preferential exposure of the {001} facet in the hydrothermal synthesis of TiO_2 nanoparticles. For example, hydrothermal treatment of titanium isopropoxide in an aqueous solution of tetrabutylammonium hydroxide and diethanolamine at 498 K yielded cubic TiO_2 particles that exposed 35% {001} facets.[19] With the aid of diethylenetriamine, solvothermal treatment of titanium isopropoxide in isopropyl alcohol produced TiO_2 nanosheets of only 3 nm thickness and the exposed fraction of the {001} facet drastically increased to 95–99%.[20] These organic amines were proposed to effectively stabilize the reactive facet and inhibit the growth of TiO_2 nanoparticles along the [001] direction. Inorganic anions were also effective in tuning the morphology of TiO_2 nanoparticles. Hydrothermal treatment of titanium isopropoxide, in the presence of $(NH_4)_2CO_3$, yielded TiO_2 truncated bipyramids that were enclosed by 35% {001} facets, in which CO_3^{2-} acted as the structure-directing agent through adsorption on the {001} facet.[21] By applying potassium titanate nanowires as precursors and urea as the capping agent, TiO_2 truncated bipyramids exposing 60% {001} facets were produced.[22] More recently, Cl^- has been reported to induce the selective exposure of the {001} facet of TiO_2 nanosheets during hydrolysis of tetrabutyl titanate ($Ti(OBu)_4$) in toluene–water bi-phase solution and the nanosheets had a thickness of 10 nm and a side length of 92 nm and exposed 82% {001} facets.[23]

In this work, we report a facile hydrothermal approach to synthesize anatase TiO_2 truncated bipyramids simply using

State Key Laboratory of Catalysis, Dalian Institute of Chemical Physics, Chinese Academy of Sciences, Dalian 116023, China. E-mail: yongli@dicp.ac.cn, shen98@dicp.ac.cn

vanadia as the structure-directing agent. By increasing the amount of vanadia in the synthetic solution, the exposed fraction of the {001} facet approached 53%. After calcination at 723 K in air, the resulting VO_x/TiO_2 truncated bipyramids effectively catalyzed the selective reduction of NO by NH_3.

Experimental section

Materials preparation

Anatase TiO_2 truncated bipyramids were synthesized by using a hydrothermal method. For the synthesis of the TiO_2-10 sample, 0.1909 g of NH_4VO_3 was dissolved in 20 ml of CH_3COOH under vigorous stirring at room temperature, then 0.5 ml of $NH_3{\cdot}H_2O$ and 5 ml of $Ti(OBu)_4$ were added gradually to produce a V/Ti molar ratio of 10. After stirring for 30 min, the light yellow mixture was transferred into a 50 ml Teflon-lined autoclave and heated at 473 K for 24 h. After cooling down to room temperature naturally, the precipitate was centrifuged, washed thoroughly with water, and dried at 353 K for 12 h. The TiO_2-15 and TiO_2-18 samples were prepared using the same procedure but the V/Ti molar ratios were increased to appropriate values. For the catalytic tests, all samples were further calcined at 723 K in air for 2 h and the obtained samples were labeled as VO_x/TiO_2-10, VO_x/TiO_2-15 and VO_x/TiO_2-18. Elemental analysis, performed using inductively coupled plasma atomic emission spectroscopy on a Plasma-Spec-II spectrometer, determined that the actual loading of vanadia was 10%, 15% and 18% by weight, respectively.

Characterization

X-ray powder diffraction (XRD) patterns were recorded with a D/Max-2500/PC diffractometer (Rigaku) using a nickel-filtered Cu Kα (λ = 0.15418 nm) radiation source that was operated at 40 kV and 200 mA. Nitrogen adsorption–desorption isotherms were recorded at 77 K using an ASAP 2000 instrument (Micromeritics). Before measurement, the sample was degassed at 573 K for 4 h. The specific surface area was calculated by multipoint Brunauer–Emmett–Teller (BET) analysis of N_2 adsorption isotherms. Transmission electron microscopy (TEM) images were recorded with a FEI Tecnai G^2 Spirit microscope operated at 120 kV. High resolution TEM (HRTEM) images were taken using a FEI Tecnai G^2 F30S-Twin microscope operated at 300 kV. The specimen was prepared by ultrasonically dispersing the sample powder in ethanol, and droplets of the suspension were deposited on a carbon-coated copper grid and dried in air. Scanning electron microscopy (SEM) images were taken with a Quanta 200 FEG scanning electron microscope. UV-visible diffuse reflectance spectra were recorded in the range of 200–900 nm with a spectrophotometer (JASCO-550, Japan) using $BaSO_4$ as the reference. X-ray photoelectron spectra (XPS) were recorded with a VG ESCALAB MK-II spectrometer with Al Kα radiation. The powder sample was pressed into a thin disc and mounted on a sample rod placed in the analysis chamber, where the spectra of V2p, Ti2p, and O1s were recorded. The charging effect was corrected by adjusting the binding energy of C1s to 284.6 eV. Visible Raman spectra were recorded at room temperature using a Jobin-Yvon U1000 scanning double monochromator with a spectral resolution of 4 cm^{-1}. A single-frequency line at 532 nm from a DPSS laser was used as the excitation source.

Catalytic measurements

Selective catalytic reduction of NO by NH_3 was performed with a continuous-flow fixed-bed quartz reactor at atmospheric pressure. 100 mg of the catalyst (40–60 mesh) was pretreated with a 3.0 vol.% O_2/He mixture (60 mL min^{-1}) at 673 K for 0.5 h. After cooling down to the desired temperature, a gas stream containing 1000 ppm NO, 1000 ppm NH_3, 3 vol.% O_2 and He with a flow rate of 120 mL min^{-1} was introduced. The concentrations of nitrogen oxides and nitrogen in the inlet and outlet streams were continuously detected by using a NO/NO_x analyzer and a mass spectrometer.

Results and discussion

TiO_2 truncated bipyramids

Fig. 1 shows the XRD pattern of the TiO_2-10 sample. All diffraction lines were ascribed to anatase TiO_2 (JCPDS # 21-1272). Compared with the standard card, however, the (200) diffraction line intensified while the (004) diffraction line weakened, suggesting that the TiO_2 particles predominantly exposed the {001} facet because of the reduced size along the [001] direction and the enlarged size along the [100] axis.[24,25] SEM/TEM images (Fig. 2) showed that the sample exhibited truncated bipyramids with a side length of 40 nm and a thickness of 28 nm. As viewed from the front direction, the two lattice spacings of 0.19 nm with an interfacial angle of 90° corresponded to {200} and {020} planes. The lattice spacings of 0.35 and 0.47 nm with an interfacial angle of 70°, viewed from the side, were ascribed to {011} and {002} planes, respectively. The interfacial angle of 68.3° was theoretically identical to the angle between the {001} and {101} facets of anatase TiO_2.[14] The selective area electron diffraction pattern confirmed the single-crystalline nature of the sample. Therefore, the TiO_2 truncated bipyramids were enclosed by eight {101} facets on the isosceles trapezoidal

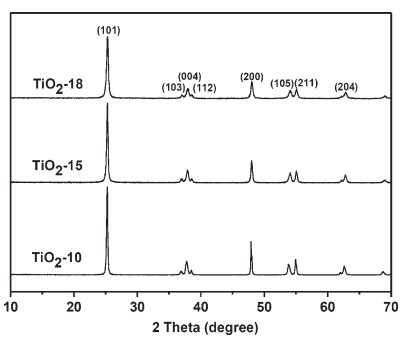

Fig. 1 XRD patterns of TiO_2 truncated bipyramids.

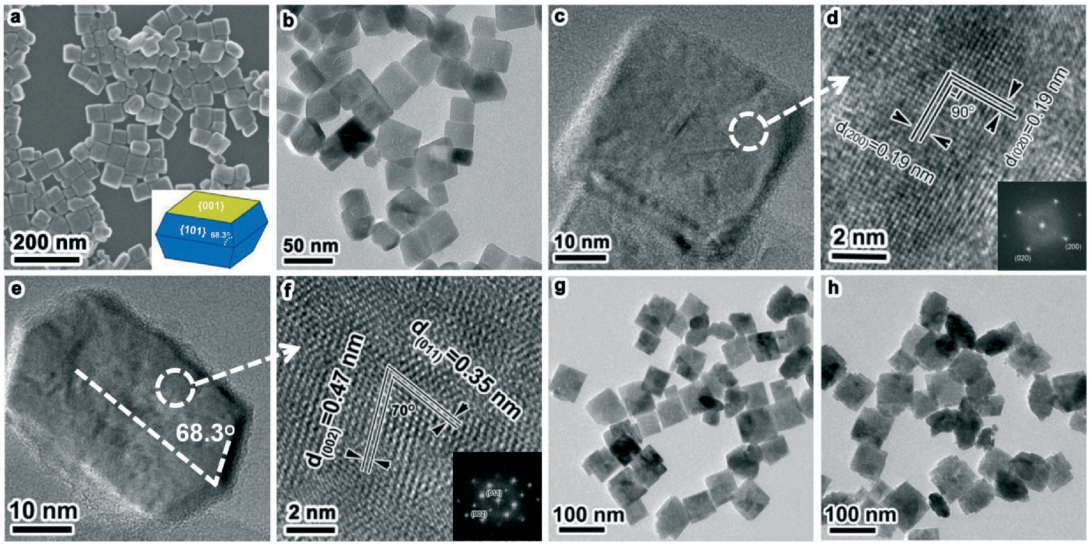

Fig. 2 SEM/TEM images of TiO_2-10 (a–f), TiO_2-15 (g) and TiO_2-18 (h) truncated bipyramids.

surface and two {001} facets on the square surface, and the surface area of the {001} facet approached about 36% of the total surface area.

As the V/Ti ratio of the synthetic solution was further increased, the obtained TiO_2-15 and TiO_2-18 samples which exhibited truncated bipyramids (Fig. 2) still gave the typical diffraction lines of anatase TiO_2 (Fig. 1), but their sizes increased to 70 and 85 nm. The exposed fraction of the {001} facet increased as well to 44% and 53%, respectively. These results demonstrate that anatase TiO_2 truncated bipyramids selectively exposing the {001} facet could be hydrothermally synthesized using vanadia as the capping agent.

Formation pathway of TiO_2 truncated bipyramids

Control experiments were conducted to determine the role of NH_4VO_3 in the synthetic solution. As shown in Fig. 3, hydrothermal synthesis in the absence of NH_4VO_3 yielded irregular nanoparticles of 35–50 nm. As NH_4VO_3 was replaced with an equal amount of NH_4Cl, large TiO_2 particles of 60–150 nm were obtained. Interestingly, substituting NH_4VO_3 with an equal amount of $NaVO_3$ produced TiO_2 truncated bipyramids of 45 nm. These results confirm that VO_3^-, instead of NH_4^+, is the key species involved in the formation of truncated bipyramids selectively exposing the reactive {001} facet. This might be due to the fact that vanadia preferentially adsorbed on the {001} facet of anatase TiO_2, which consists of low-coordinated titanium and oxygen atoms and provides strongly acidic and basic sites.[26] The formation of the V–O–Ti bridging bond, upon vanadia adsorption, would drastically lower the surface energy of the {001} facet and thus induce an epitaxial growth pattern.

The structural evolution of the products at different intervals during hydrothermal synthesis was examined by TEM and XRD measurements (Fig. 4). All precipitates gave diffraction lines of anatase TiO_2; the crystalline degree gradually increased with increasing time. The morphology of the products changed drastically. Floccule-like particles were formed at 0.5 h. Nanoparticles of 11 nm were formed and dispersed

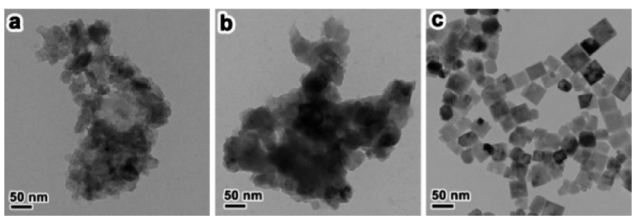

Fig. 3 TEM images of the samples prepared by varying the chemical composition of the synthetic solution: (a) without addition of NH_4VO_3, (b) substitution of NH_4VO_3 with an equivalent amount of NH_4Cl, and (c) replacement of NH_4VO_3 with an equivalent amount of $NaVO_3$. Synthesis conditions: 20 ml CH_3COOH, 5 ml $Ti(OBu)_4$, 0.5 ml $NH_3{\cdot}H_2O$, 473 K, 24 h; the V/Ti molar ratio was kept at 10% if vanadate was applied.

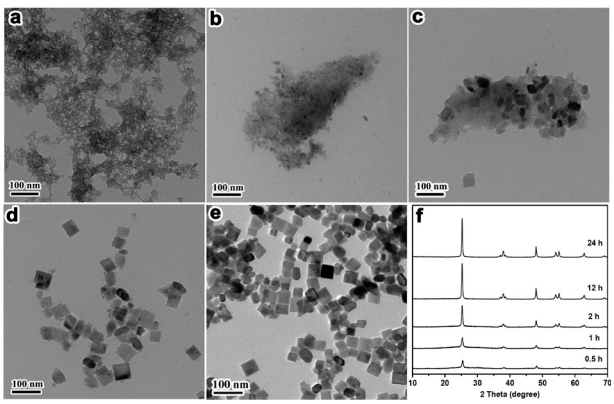

Fig. 4 TEM images (a–e) and XRD patterns (f) of the products obtained at different time intervals during synthesis: 0.5 h (a), 1 h (b), 2 h (c), 12 h (d), and 24 h (e). Synthesis conditions: 20 ml CH_3COOH, 0.5 ml $NH_3{\cdot}H_2O$, 0.1909 g NH_4VO_3, 5 ml $Ti(OBu)_4$, 473 K.

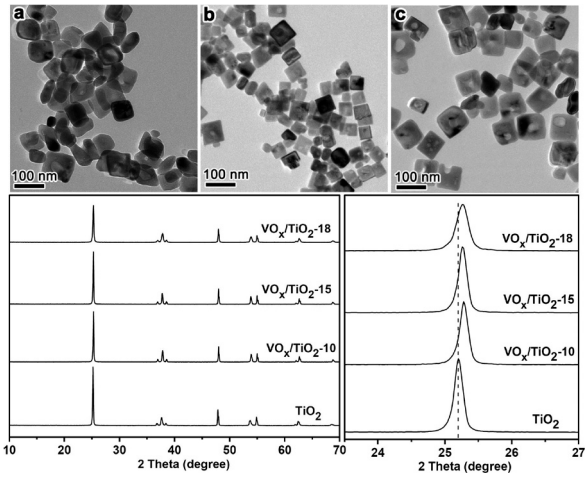

Fig. 5 TEM images and XRD patterns of (a) VO_x/TiO_2-10, (b) VO_x/TiO_2-15, and (c) VO_x/TiO_2-18 samples obtained by calcination of the as-prepared anatase TiO_2 truncated bipyramids. The reference pure anatase TiO_2 sample was obtained by calcination of the precursor in Fig. 3(a) at 723 K in air for 2 h.

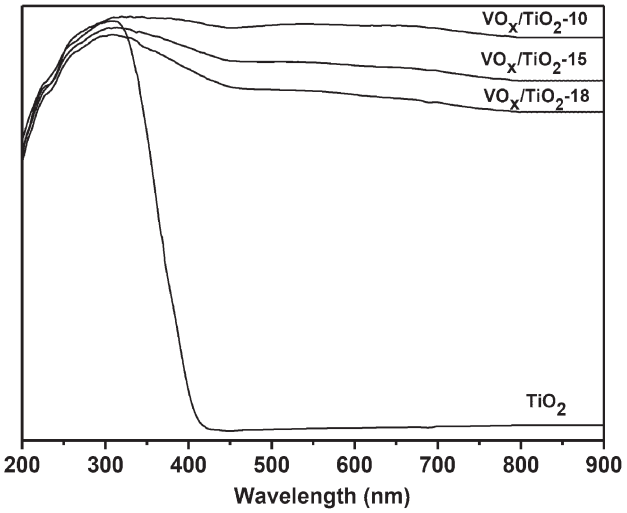

Fig. 6 UV-visible spectra of VO_x/TiO_2 samples. The reference pure anatase TiO_2 sample was obtained by calcination of the precursor in Fig. 3(a) at 723 K in air for 2 h.

on the floccule-like precipitate at 1 h, while truncated bipyramid spindles of 25 nm appeared at 2 h. When the hydrothermal time lasted for 12 h, the floccule-like particles disappeared entirely and truncated bipyramids of 35 nm were formed as the main product. At 24 h, truncated bipyramids of 40 nm were formed as the only product. This growing process could be proposed as follows: hydrolysis of $Ti(OBu)_4$ and subsequent polymerization of Ti–O–Ti linkages initially produced floccule-like particles; vanadia that strongly adsorbed on the {001} facet of the small nanoparticles induced their assembly into well-defined truncated bipyramids.

NH_3-SCR activity

VO_x/TiO_2 catalysts are industrially used for the selective reduction of NO by NH_3 to abate polluting emissions from power plants.[27–29] The as-synthesized TiO_2 truncated bipyramids were calcined at 723 K in air and were used to catalyze the selective reduction of NO by NH_3. As shown in Fig. 5, the VO_x/TiO_2 samples retained their original shape and size, but contained significant amounts of surface pores that were generated during the calcination process due to the release of water and CO_2. Their XRD patterns indicated the crystalline phase of anatase TiO_2, but the (101) diffraction line was slightly shifted toward a higher angle, as compared with that of a pure anatase TiO_2 sample. This suggests that the vanadia species incorporated into the lattice of TiO_2, and the smaller ionic radius of V^{n+} (0.054 nm for V^{5+} and 0.058 nm for V^{4+}) than that of Ti^{n+} (0.061 nm for Ti^{4+} and 0.067 nm for Ti^{3+}) reduced the crystalline cell size (Table 1).

Meanwhile, the (101) diffraction line slightly shifted as the V/Ti molar ratio of the VO_x/TiO_2 samples increased. This might be due to variation in the amount of vanadia doped into the lattice of TiO_2. UV-visible absorption spectra of the VO_x/TiO_2 samples (Fig. 6) further evidenced doping of vanadia into the TiO_2 lattice. Compared with that of a pure anatase TiO_2 sample, the absorption edge of the truncated bipyramids distinctively shifted to the visible region at 400–900 nm, primarily because of charge transfer from V^{4+} to the conduction band of TiO_2.[30]

Fig. 7 shows the XPS spectra of V2p, Ti2p and O1s in the VO_x/TiO_2 samples. The binding energies at 517.6 and 516.5 eV are attributed to V^{5+} and V^{4+} species,[31] while the binding energy at 458.5 eV is ascribed to Ti^{4+},[32] respectively. The binding energies at 530.1 and 531.2 eV are assigned to the lattice (O_α) and defect oxygen species (O_β),[33] respectively. Quantitative analysis of the XPS profiles verified that the surface molar ratio of V/Ti was 2.8% for VO_x/TiO_2-10, 9.1% for VO_x/TiO_2-15, and 12.9% for VO_x/TiO_2-18 (Table 1), while the corresponding bulk V/Ti molar ratio,

Table 1 Structural parameters and NH_3-SCR activity of the VO_x/TiO_2 catalysts

Sample	V/Ti[a] (mol%)	Surface molar content[b] (%)			Surface area ($m^2\ g^{-1}$)	Lattice parameter (nm)		Reaction rate[c] (mol $g^{-1}\ s^{-1}$)	TOF[d] (s^{-1})
		V	Ti	O		*a*	*c*		
VO_x/TiO_2-10	9.9	0.9	32.3	66.8	64.3	0.3789	0.9513	2.3×10^{-8}	2.1×10^{-5}
VO_x/TiO_2-15	14.9	2.9	31.9	65.2	53.9	0.3792	0.9509	7.8×10^{-7}	4.8×10^{-4}
VO_x/TiO_2-18	19.1	4.1	31.7	64.2	45.1	0.3793	0.9508	1.7×10^{-6}	8.9×10^{-4}

[a] Determined by ICP analysis. [b] Determined from the XPS profiles in Fig. 7. [c] Measured at 473 K with an NO conversion below 15%. [d] Calculated by taking the actual loading of vanadia into account.

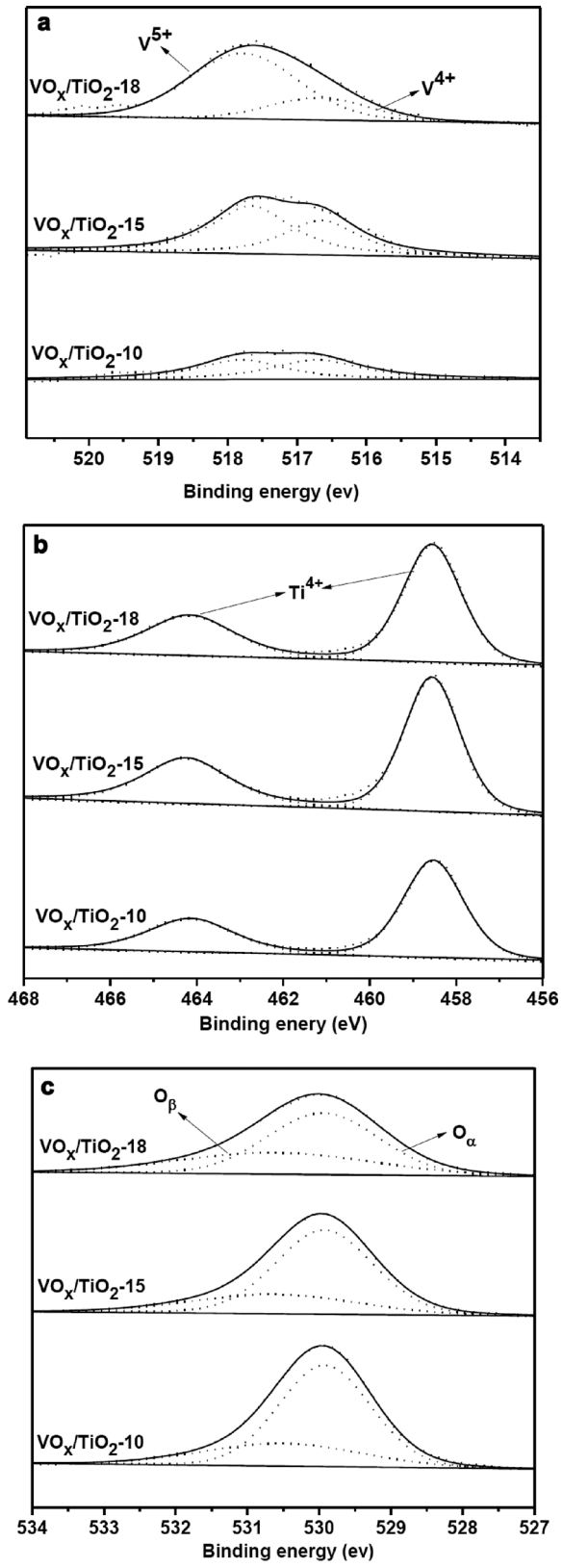

Fig. 7 XPS spectra of VO_x/TiO_2 samples: (a) V2p3/2, (b) Ti2p3/2, and (c) O1s.

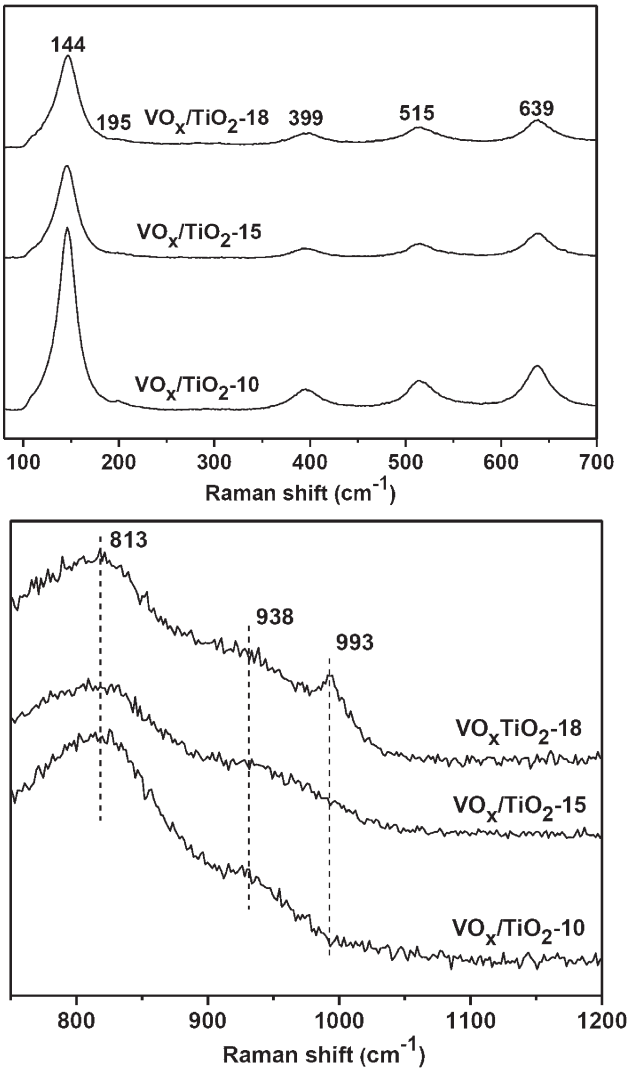

Fig. 8 Raman spectra of VO_x/TiO_2 samples.

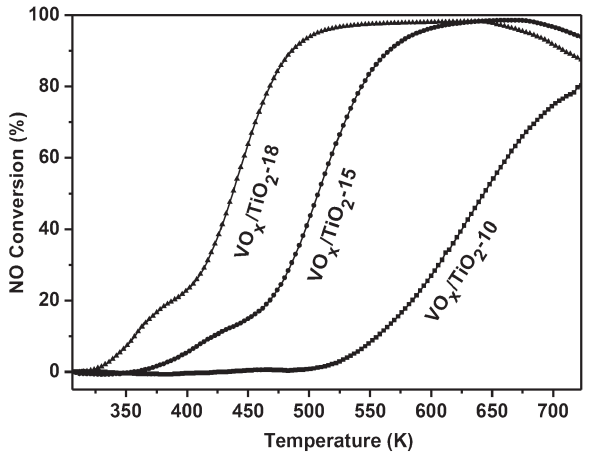

Fig. 9 NO conversion on the VO_x/TiO_2 samples as a function of temperature in selective reduction of NO by ammonia. Reaction conditions: 100 mg catalyst, 1000 ppm NH_3/1000 ppm NO/3% O_2/He, 72 000 ml g^{-1} h^{-1}.

measured by ICP, was 9.9%, 14.9% and 19.1%, respectively. It seems that the lower V/Ti molar ratio favored the doping of vanadia into the lattice of TiO_2, whereas more vanadia species existed on the surface of the samples at higher V/Ti molar ratios, which is in accordance with the XRD patterns in Fig. 5.

Fig. 8 shows the Raman spectra of the VO_x/TiO_2 samples. The intensity of the symmetric stretching vibration of O–Ti–O, typically shown at 144 cm^{-1} in anatase TiO_2,[24] gradually decreased with increasing content of vanadia. This is caused by the enhanced exposure of the {001} facet with increasing VO_x doping. The {001} facet of TiO_2 is terminated with five-fold Ti atoms (Ti_{5C}) and two-fold O atoms (O_{2C}), and such an atomic configuration decreases the number of symmetric stretching vibrations of O–Ti–O and hence weakens their intensity.[14,24] The broad peaks at 813 and 938 cm^{-1} were assigned to the asymmetric stretching modes of V–O–V and terminal V═O.[34–38] This means that surface vanadia exists mainly as polymeric species. However, an additional peak at 993 cm^{-1} over the VO_x/TiO_2-18 sample appeared, indicating the presence of crystalline V_2O_5.[39–41] That is, most vanadia species were incorporated into the TiO_2 lattice for the VO_x/TiO_2-10 sample, whereas more surface vanadia and a small amount of crystalline V_2O_5 were formed on TiO_2 truncated bipyramids at higher vanadia contents.

Fig. 9 shows the NO conversions on the VO_x/TiO_2 truncated bipyramids in NH_3-SCR. The VO_x/TiO_2-10 catalyst showed an NO conversion of 50% at 643 K and 80% at 703 K. With further increasing vanadia content, the catalytic activity increased significantly; the VO_x/TiO_2-18 catalyst provided an NO conversion of 50% at 433 K and 90% at 476 K. The reaction rate measured at 473 K (Table 1) increased from 2.3×10^{-8} mol g^{-1} s^{-1} over the VO_x/TiO_2-10 sample to 1.7×10^{-6} mol g^{-1} s^{-1} on the VO_x/TiO_2-18 catalyst, while the corresponding turnover frequency, based on the actual loading of VO_x, increased remarkably from 2.1×10^{-5} to 8.9×10^{-4} s^{-1}. Since crystalline V_2O_5 is usually less active for NH_3-SCR,[42] the higher activity of the VO_x/TiO_2-18 catalyst might be related to the presence of surface vanadia species on the TiO_2 truncated bipyramids. The relatively lower activity of the VO_x/TiO_2-10 catalyst was caused by the incorporation of most vanadia species into the TiO_2 lattice.

Conclusions

Anatase TiO_2 truncated bipyramids with preferential exposure of the reactive {001} facet were successfully synthesized using only vanadia as the structure-directing agent. The exposure of the {001} facet approached 53% upon increasing the amount of vanadia, which strongly adsorbed on the reactive facet and induced the construction of truncated bipyramids. Calcination of the as-prepared truncated bipyramids yielded VO_x/TiO_2 catalysts, in which vanadia species were partially incorporated into the TiO_2 lattice. The surface and crystalline vanadia species on the surface of TiO_2 truncated bipyramids were active for the selective reduction of NO by ammonia.

Acknowledgements

This work was supported by the National Natural Science Foundation of China (21025312 and 21103177) and the National Key Basic Research Program of China (2013CB933100).

Notes and references

1 Q. Kuang, X. Wang, Z. Y. Jiang, Z. X. Xie and L. S. Zheng, *Acc. Chem. Res.*, 2014, **47**, 308–318.
2 Y. Li and W. J. Shen, *Chem. Soc. Rev.*, 2014, **43**, 1543–1574.
3 W. X. Huang and Y. X. Gao, *Catal. Sci. Technol.*, 2014, **4**, 3772–3784.
4 G. Liu, J. C. Yu, G. Q. Lu and H. M. Cheng, *Chem. Commun.*, 2011, **47**, 6763–6783.
5 C. Z. Wen, H. B. Jiang, S. Z. Qiao, H. G. Yang and G. Q. Lu, *J. Mater. Chem.*, 2011, **21**, 7052–7061.
6 W. J. Ong, L. L. Tan, S. P. Chai, S. T. Yong and A. R. Mohamed, *Nanoscale*, 2014, **6**, 1946–2008.
7 H. Xu, S. Ouyang, L. Q. Liu, P. Reunchan, N. Umezawa and J. H. Ye, *J. Mater. Chem. A*, 2014, **2**, 12642–12661.
8 G. Liu, H. G. Yang, J. Pan, Y. Q. Yang, G. Q. Lu and H. M. Cheng, *Chem. Rev.*, 2014, **114**, 9559–9612.
9 U. Diebold, *Surf. Sci. Rep.*, 2003, **48**, 53–229.
10 X. Q. Gong and A. Selloni, *J. Phys. Chem. B*, 2005, **109**, 19560–19562.
11 Q. X. Deng, M. D. Wei, X. K. Ding, L. L. Jiang, K. W. Wei and H. S. Zhou, *J. Cryst. Growth*, 2010, **312**, 213–219.
12 J. Zhang, L. S. Qian, L. X. Yang, X. Tao, K. P. Su, H. B. Wang, J. H. Xia and Z. G. Jia, *Appl. Surf. Sci.*, 2014, **311**, 521–528.
13 M. Lazzeri, A. Vittadini and A. Selloni, *Phys. Rev. B: Condens. Matter Mater. Phys.*, 2001, **63**, 155409 (9 PP).
14 H. G. Yang, C. H. Sun, S. Z. Qiao, J. Zou, G. Liu, S. C. Smith, H. M. Cheng and G. Q. Lu, *Nature*, 2008, **453**, 638–641.
15 C. Z. Wen, J. Z. Zhou, H. B. Jiang, Q. H. Hu, S. Z. Qiao and H. G. Yang, *Chem. Commun.*, 2011, **47**, 4400–4402.
16 Q. Q. Shi, Y. Li, E. S. Zhan, N. Ta and W. J. Shen, *CrystEngComm*, 2014, **16**, 3431–3437.
17 X. K. Ding, H. C. Ruan, C. Z. Zheng, J. Yang and M. D. Wei, *CrystEngComm*, 2013, **15**, 3040–3044.
18 X. G. Han, Q. Kuang, M. S. Jin, Z. X. Xie and L. S. Zheng, *J. Am. Chem. Soc.*, 2009, **131**, 3152–3153.
19 N. Roy, Y. Sohn and D. Pradhan, *ACS Nano*, 2013, **7**, 2532–2540.
20 J. S. Chen, Y. L. Tan, C. M. Li, Y. L. Cheah, D. Y. Luan, S. Madhavi, F. Y. C. Boey, L. A. Archer and X. W. Lou, *J. Am. Chem. Soc.*, 2010, **132**, 6124–6130.
21 N. Sutradhar, A. K. Biswas, S. K. Pahari, B. Ganguly and A. B. Panda, *Chem. Commun.*, 2014, **50**, 11529–11532.
22 X. G. Han, X. Wang, S. F. Xie, Q. Kuang, J. J. Ouyang, Z. X. Xie and L. S. Zheng, *RSC Adv.*, 2012, **2**, 3251–3253.
23 X. L. Cheng, M. Hu, R. Huang and J. S. Jiang, *ACS Appl. Mater. Interfaces*, 2014, **6**, 19176–19183.

24 F. Tian, Y. P. Zhang, J. Zhang and C. X. Pan, *J. Phys. Chem. C*, 2012, **116**, 7515–7519.
25 C. Hu, X. Zhang, W. T. Li, Y. Yan, G. C. Xi, H. F. Yang, J. F. Li and H. Bai, *J. Mater. Chem. A*, 2014, **2**, 2040–2043.
26 Y. J. Du, Z. H. Li and K. N. Fan, *Surf. Sci.*, 2012, **606**, 956–964.
27 G. Busca, L. Lietti, G. Ramis and F. Berti, *Appl. Catal., B*, 1998, **18**, 1–36.
28 S. Roy, M. S. Hegde and G. Madras, *Appl. Energy*, 2009, **86**, 2283–2297.
29 P. Granger and V. I. Parvulescu, *Chem. Rev.*, 2011, **111**, 3155–3207.
30 K. Bhattacharyya, S. Varma, A. K. Tripathi, S. R. Bharadwaj and A. K. Tyagi, *J. Phys. Chem. C*, 2008, **112**, 19102–19112.
31 H. Y. Zhao, S. Bennici, J. Y. Shen and A. Auroux, *J. Catal.*, 2010, **272**, 176–189.
32 D. W. Kwon, K. H. Park and S. C. Hong, *Appl. Catal., A*, 2013, **451**, 227–235.
33 S. L. Zhang, H. Y. Li and Q. Zhong, *Appl. Catal., A*, 2012, **435**, 156–162.
34 G. T. Went, L. J. Leu, S. J. Lombardo and A. T. Bell, *J. Phys. Chem.*, 1992, **96**, 2235–2241.
35 G. T. Went, L. J. Leu and A. T. Bell, *J. Catal.*, 1992, **134**, 479–491.
36 U. Scharf, M. Schneider, A. Baiker and A. Wokaun, *J. Catal.*, 1994, **149**, 344–355.
37 A. Khodakov, B. Olthof, A. T. Bell and E. Iglesia, *J. Catal.*, 1999, **181**, 205–216.
38 A. Christodoulakis, M. Machli, A. A. Lemonidou and S. Boghosian, *J. Catal.*, 2004, **222**, 293–306.
39 T. Machej, J. Haber, A. M. Turek and I. E. Wachs, *Appl. Catal.*, 1991, **70**, 115–128.
40 G. T. Went, L. J. Leu and A. T. Bell, *J. Catal.*, 1992, **134**, 492–505.
41 D. A. Bulushev, L. Kiwi-Minsker, V. I. Zaikovskii and A. Renken, *J. Catal.*, 2000, **193**, 145–153.
42 U. S. Ozkan, Y. P. Cai and M. W. Kumthekar, *Appl. Catal., A*, 1993, **96**, 365–381.

